# Energetic aspects of the Reynolds analogy in rough-wall turbulent forced convection

Journal of Physics: Conference Series **3173** (2026) 012020 doi:10.1088/1742-6596/3173/1/012020

# Energetic aspects of the Reynolds analogy in rough-wall turbulent forced convection

**Francesco Secchi[1], Davide Gatti[1], Ugo Piomelli[2] and Bettina Frohnapfel[1]**

[1]Institute of Fluid Mechanics, Karlsruhe Institute of Technology, Karlsruhe, Germany
[2]Department of Mechanical and Materials Engineering, Queen's University, Kingston, Canada

E-mail: francesco.secchi@kit.edu

**Abstract.** This work investigates the Reynolds analogy in turbulent forced convection over rough walls using an energetic framework. Extending the analysis of Secchi et al. [1], we relate momentum and scalar transfer to the integral dissipation rates of mechanical energy and the squared scalar field, examining how these quantities depend on the method used to drive the flow. Direct numerical simulations of rough-wall channel flows at friction Reynolds numbers up to $Re_\tau = 540$ are rescaled to compare three driving strategies: constant pressure gradient (CPG), constant flow rate (CFR), and constant power input (CPI). For each flow driving strategy appropriate indexes for measuring the net momentum and scalar transfer are identified and their relationships to the integral dissipation rates of mechanical and squared scalar field are investigated.

## 1 Introduction

The Reynolds analogy describes the similarity between momentum and scalar transfer between a flow and a solid surface. In practical applications, this analogy often breaks down due to the action of the pressure field, which introduces a momentum exchange mechanism that does not directly affect the scalar transfer. A classical example that exhibits non-analogous momentum and scalar transfer is represented by turbulent flows over surface roughness. In particular, the extent to which momentum and scalar transfer differ depends on the flow regime.

When the characteristic scales of the flow and surface roughness are sufficiently separated, the flow does not sense the roughness and behaves as if over a smooth surface. This regime is referred to as hydrodynamically smooth. As the roughness length scale begins to overlap with the flow scale, the system enters the transitionally rough regime. In this regime, both mean momentum and scalar exchange are enhanced, though through different mechanisms: roughness elements introduce a pressure drag that affects the momentum transfer without equally affecting the scalar one. Consequently, even when molecular diffusivities of momentum and scalar are similar, the roughness-induced augmentation of momentum transfer exceeds that of scalar transfer. This disparity becomes more pronounced in the fully rough regime, where pressure drag dominates the momentum exchange.

Despite the clear current understanding of the phenomenological scenario behind dissimilar momentum and scalar transfer, a predictive model for scalar transfer enhancement due to roughness remains elusive [2]. In order to characterize the momentum and scalar transfer dissimilarity, it seems beneficial to quantify the effects of flow phenomena on the net momentum and scalar transfer. For instance, in smooth wall flows, exact relationships exist between the non-dimensional momentum and scalar wall fluxes, *i.e.* the friction and scalar transfer coefficients, and the Reynolds shear stresse and turbulent

wall-normal flux, respectively [3, 4]. These relationships enable the quantification of the turbulent fluctuations contributions to the momentum and scalar wall fluxes. Similarly, in [5] and [6], momentum and scalar transfer laws as functions of the Reynolds number are deduced based on an analysis of the integral dissipation of the turbulent kinetic energy and scalar variance in smooth wall flows.

The recent work of Secchi et al. [1] generalizes such an approach and applies it to the analysis of rough wall flows. In particular, the analysis starts by considering the similarity between the equations governing, in statistically stationary flows, the time-averaged mechanical energy, given by the sum of kinetic energy and pressure work, and the squared magnitude of the scalar concentration. For channel flow configurations, the integral balance of these equations reduces to a link between indexes of the mean momentum and scalar transfer and the integral mean of the dissipation rates of mechanical energy and squared scalar field in the channel. In particular, under constant pressure gradient (CPG) conditions, these relationships are used to relate the viscous units-scaled mean bulk velocity and scalar to the non-dimensional integral dissipations rates. In [1] this fact is used to investigate how momentum and scalar transfer respond differently to the presence of surface roughness based on the analysis of the dissipation rates of mechanical energy and the squared scalar field.

However, CPG is not the only possibility for driving the flow in a fully developed channel. A common alternative consists in prescribing a constant flow rate (CFR), whereby increases in the mean momentum transfer in the rough channel manifest themselves as higher mean pressure gradients required to drive the flow at the prescribed flow rate. A less common approach is that of prescribing a constant power input (CPI) to the system. In this case increases in the mean momentum transfer can equivalently be measured through increases in the mean momentum wall flux and corresponding decreases in the mean flow rate.

While each approach provides a meaningful description of the physics of the flow, the flow statistics of one single flow configuration do not depend on the particular strategy adopted to drive the flow through the channel [7]. However, significant care must be taken in the interpretation of the data for the comparison of different flow configuration or for the comparison between momentum and scalar transfer under different driving conditions. This observation becomes particularly relevant when momentum and scalar transfer are assessed through higher-order statistics such as the dissipation rates of mechanical energy and of the squared scalar field.

This work applies the energetic approach [1] to assess momentum and scalar transfer across different flow-driving strategies, providing a clear framework for such evaluations. This is achieved by a simple rescaling of the direct numerical simulation (DNS) data in [1] to enable the evaluation of the roughness-induced momentum and scalar transfer increase under the CFR and CPI flow driving strategies. The theoretical framework is presented in section 2 for each driving strategy, whereas its application to the DNS is reported in section 3.

## 2 Theoretical framework

In this work we consider an incompressible flow of a Newtonian fluid with constant properties. The passive scalar field $\vartheta$ is assumed to be governed by an unsteady convection diffusion equation. In this context, analogous momentum and scalar transfer is typically inferred from the formal similarity between the fluid momentum balance equation and the equation governing the passive scalar field, neglecting the pressure gradient in the momentum equation. However, the vectorial nature of the momentum balance complicates direct comparison with the scalar equation. A natural solution is to establish an analogy between scalar quantities; in this context, kinetic energy is an ideal candidate, as it reflects the magnitude of momentum and evolves according to a scalar equation. As shown in [1], the latter can be written as:

$$\frac{\partial \mathcal{K}}{\partial t} + u_i \frac{\partial \mathcal{B}}{\partial x_i} = f_j u_j + \nu \frac{\partial^2 \mathcal{B}}{\partial x_i \partial x_i} - \nu \omega_i \omega_i, \tag{1}$$

where $\mathcal{K} = u_i u_i/2$ is the kinetic energy, $u_i$ is the $i$th velocity component (summation over repeated indices is implied), $\nu$ is the kinematic viscosity of the fluid, and $\omega_i$ is the $i$th vorticity component. A new character appears in the equation above; this is the total mechanical energy, $\mathcal{B} = \mathcal{K} + p/\rho$, given by the sum of kinetic energy and pressure work (the pressure is denoted with $p$, and $\rho$ is the fluid density,).

For the scalar field, an equation analogous to (1) can be found for the squared scalar field, $\mathcal{G} = \vartheta^2/2$, which, in a similar fashion to the kinetic energy, represents the squared magnitude of the scalar concentration. As shown in [1], the squared scalar field is governed by the following equation:

$$\frac{\partial \mathcal{G}}{\partial t} + u_i \frac{\partial \mathcal{G}}{\partial x_i} = q\vartheta + \alpha \frac{\partial^2 \mathcal{G}}{\partial x_i \partial x_i} - \alpha \frac{\partial \vartheta}{\partial x_i} \frac{\partial \vartheta}{\partial x_i}, \tag{2}$$

where $q$ is the source term in the passive scalar equation, and $\alpha$ is the molecular diffusivity of the scalar.

Under statistically stationary conditions, time averaging eliminates the time derivative terms on the left-hand side of equations (1) and (2), yielding two structurally analogous equations for $\mathcal{B}$ and $\mathcal{G}$. Using an overline to denote time averaging, these equations become:

$$0 = \overline{f_j u_j} + \frac{\partial}{\partial x_i}\left(-\overline{\mathcal{B} u_i} + \nu \frac{\partial \overline{\mathcal{B}}}{\partial x_i}\right) - \nu \overline{\omega_i \omega_i}, \tag{3}$$

$$0 = \overline{q\vartheta} \quad + \frac{\partial}{\partial x_i}\left(-\overline{\mathcal{G} u_i} + \alpha \frac{\partial \overline{\mathcal{G}}}{\partial x_i}\right) - \alpha \overline{\frac{\partial \vartheta}{\partial x_i}\frac{\partial \vartheta}{\partial x_i}}. \tag{4}$$

Equations (3) and (4) highlight that $\overline{\mathcal{B}}$ and $\overline{\mathcal{G}}$ are governed by similar physical processes; differences in their time-averaged distributions might arise due to differences in the external forcing fields, $f_j$ and $q$, in the molecular diffusivities, $\nu$ and $\alpha$, and in the dissipation rates, $\nu\overline{\omega_i\omega_i}$ and $\alpha\overline{\vartheta_{,i}\,\vartheta_{,i}}$ (the comma notation is used to indicate partial differentiation, *i.e.* $\frac{\partial \cdot}{\partial x_i} = (\cdot)_{,i}$). In particular, as noted in [1], under similar external forcing conditions, and for a fluid having a Prandtl number close to unity, dissimilarities in the mean distributions of mechanical energy and squared scalar field arise from dissimilarities in their dissipation rates, $\nu\overline{\omega_i\omega_i}$ and $\alpha\overline{\vartheta_{,i}\,\vartheta_{,i}}$.

### *2.1 Fully developed channel flows*

We consider a fully developed turbulent channel flow between two parallel plates separated by a distance $2\delta$. The channel walls can be either smooth or rough. The flow is driven along the streamwise direction $x = x_1$ using a uniform pressure gradient $f = f_j\delta_{1j}$. The spanwise and wall normal directions are denoted, respectively, with $y = x_2$ and $z = x_3$. No-slip velocity boundary conditions apply on the impermeable walls of the channel for the velocity field. The scalar field is assumed to have Dirichlet boundary conditions $\vartheta = 0$ on the two channel walls and is driven by a uniform scalar source term $q$.

Under these assumptions, integration of equations (3) and (4) in the channel volume, $\mathcal{V}$, results in the following integral balances:

$$\overline{fU}_b = \frac{1}{\mathcal{V}}\int_{\mathcal{V}} \nu\overline{\omega_i\omega_i}\,\mathrm{d}\mathcal{V}, \tag{5}$$

$$\overline{q\Theta}_b = \frac{1}{\mathcal{V}}\int_{\mathcal{V}} \alpha\overline{\vartheta_{,i}\,\vartheta_{,i}}\,\mathrm{d}\mathcal{V}, \tag{6}$$

where $\overline{U}_b$ and $\overline{\Theta}_b$ denote, respectively, the mean bulk velocity and scalar in the channel.

The left-hand side of equation (5) represents the total power exerted by the flow, which, under statistically stationary conditions, must balance the mechanical energy dissipated within the channel volume. Similarly, the product of the volumetric scalar source and the mean bulk scalar must equal the bulk dissipation of $\mathcal{G}$. Equations (5) and (6) relate integral quantities, such as total flow power, to field quantities like the dissipation rate. Moreover, these relationships can be further refined to connect wall fluxes with bulk dissipation fields.

## 3 Numerical results

In order to showcase the application of the framework presented in section 2, the DNS data [1] are going to be used in this section. The numerical simulations reproduce two cases of fully developed turbulent channel flow over rough walls, corresponding to selected configurations studied in [8, 9, 10, 11]. In one case, the flow is transitionally rough but close to smooth-wall conditions, with a roughness Reynolds number $k^+ = 15$. A + superscript denotes normalization based on the friction velocity, $u_\tau = (\tau_w/\rho)^{1/2}$, and $\nu$. The mean wall shear stress is indicated with $\tau_w$. In the other case, the flow approaches fully rough conditions, with $k^+ = 90$. The roughness geometry is derived from a scanned grit-blasted surface and is statistically homogeneous in the wall-parallel directions. The physical roughness height is $k = \delta/12$ for the $k^+ = 15$ case and $k = \delta/6$ for the $k^+ = 90$ case. The corresponding friction Reynolds numbers are $Re_\tau = 180$ and $Re_\tau = 540$, respectively (the friction Reynolds number is defined as $Re_\tau = u_\tau\delta/\nu$). An additional smooth wall channel flow simulation at $Re_\tau = 180$ is also considered for reference. All simulations assume a unit Prandtl number, namely $Pr = \nu/\alpha = 1$. Details about the numerical method, the resolution, and the validation of the available results can be found in [1].

### *3.1 Constant pressure gradient (CPG)*

A common method for maintaining a flow rate in a channel is to prescribe a constant pressure gradient (CPG) between the inlet and outlet, which corresponds to imposing a constant and uniform forcing term $\overline{f} = f$ to the mean momentum balance, or, equivalently, to a constant mean momentum wall flux. The appropriate velocity scale for making the problem non-dimensional is the friction velocity, defined as $u_\tau = (\tau_w/\rho)^{1/2} = (f\delta)^{1/2}$. Using the viscous length scale, $\delta_\nu = \nu/u_\tau$, as the characteristic length, the integral energy balance (5) becomes:

$$\overline{U}_b^+ = \frac{Re_\tau}{\mathcal{V}^+} \int_{\mathcal{V}^+} \overline{\omega_i^+ \omega_i^+}\, \mathrm{d}\mathcal{V}^+. \tag{7}$$

The strategy for forcing the scalar field, analogous to the CPG momentum forcing, involves prescribing a constant and uniform source term, $\overline{q} = q$. This is implicitly equivalent to setting a wall scalar flux, $q_w$. Under these conditions, the appropriate scalar scale for non-dimensionalization is the friction scalar, defined as $\vartheta_\tau = \alpha q_w/u_\tau = \delta q/u_\tau$. A viscous length scale for scalar transport is given by $\delta_\alpha = \alpha/u_\tau$, which is related to the momentum-based viscous length scale by $\delta_\alpha = \delta_\nu/Pr$, where $Pr = \nu/\alpha$ is the Prandtl number, representing the ratio of momentum to scalar molecular diffusivities. The non-dimensional form of (6) becomes:

$$\overline{\Theta}_b^+ = \frac{Pe_\tau}{\mathcal{V}^\#} \int_{\mathcal{V}^\#} \overline{\vartheta^+{}_{,i^\#}\, \vartheta^+{}_{,i^\#}}\, \mathrm{d}\mathcal{V}^\# = \frac{Re_\tau}{Pr\mathcal{V}^+} \int_{\mathcal{V}^+} \overline{\vartheta^+{}_{,i^+}\, \vartheta^+{}_{,i^+}}\, \mathrm{d}\mathcal{V}^+, \tag{8}$$

where $Pe_\tau = PrRe_\tau$ is the friction Péclet number and a $\#$ superscript denotes lengths made dimensionless using $\delta_\alpha$. Note that for a unit Prandtl number, $\delta_\alpha = \delta_\nu$.

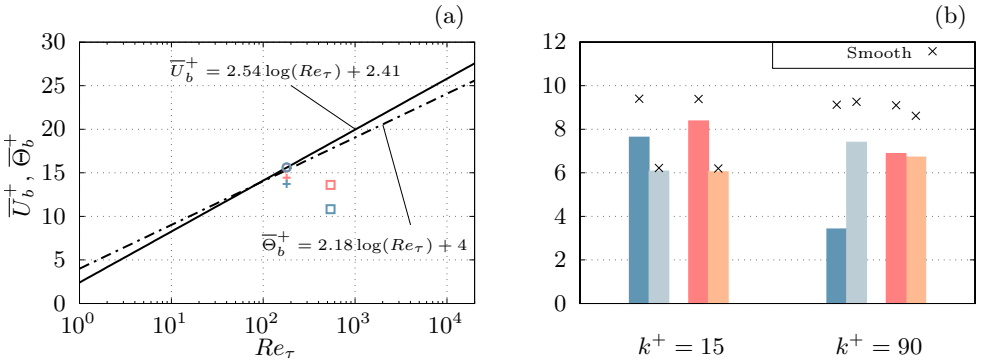


Figure 1: (a) Mean bulk velocity (blue) and scalar (red) as functions of the friction Reynolds number. Smooth wall, circle markers; rough wall $k^+ = 15$, cross markers; rough wall $k^+ = 90$, square markers. (b) Mean and turbulent contributions to the volume-averaged dissipation rates. , $Re_\tau \mathcal{E}^{m+}$; , $Re_\tau \mathcal{E}^{t+}$; , $Re_\tau \mathcal{E}_\mathcal{G}^{m+}/Pr$; , $Re_\tau \mathcal{E}_\mathcal{G}^{t+}/Pr$. Figure adapted from [1].

Under the CPG scaling, the mean bulk velocity and scalar are representative indexes of the momentum scalar transfer similarity. In fact, in the literature a quantification of such a similarity is computed using the Reynolds analogy factor, measuring the ratio between the scalar transfer coefficient, $C_h$, and the friction coefficient, $C_f$. For the CPG scaling, the Reynolds analogy factor can be computed as, $RA = 2C_h/C_f = \overline{U}_b^+/\overline{\Theta}_b^+$ (for instance, see [1]).

Figure 1(a) presents the computed values of $\overline{U}_b^+$ and $\overline{\Theta}_b^+$ as functions of the friction Reynolds number for all simulated cases. For reference, the expected logarithmic trends for smooth-wall channel flow are also shown, based on the correlations in [5, 6]. For the smooth wall data, as the friction Reynolds number increases, so do the dimensionless mean bulk velocity and scalar achieved in the channel. The presence of surface roughness enhances both momentum and scalar transfer, leading to a reduction in the bulk velocity and scalar in wall units in comparison to the smooth wall reference values at matched $Re_\tau$. As a result, the rough-wall data consistently fall below the smooth-wall asymptotic curves. In particular, it is evident how the mean bulk velocity decreases more significantly than the mean bulk scalar, indicating a clear dissimilarity between the mean momentum and scalar transfer.

The CPG scaling allows for the computation of the mean bulk velocity and scalar from the mean bulk dissipation rates of mechanical energy and squared scalar field, as given in equations (7) and (8), respectively. This approach can be leveraged to separate the contributions of the mean and turbulent flow to overall momentum and scalar transport. In particular, following [1], upon applying the classical Reynolds decomposition to the integral dissipation rates on the right-hand side of equations (7) and (8), the mean bulk velocity and scalar can be written as:

$$\overline{U}_b^+ = Re_\tau \mathcal{E}^{m+} + Re_\tau \mathcal{E}^{t+}, \tag{9}$$

$$\overline{\Theta}_b^+ = \frac{Re_\tau}{Pr} \mathcal{E}_\mathcal{G}^{m+} + \frac{Re_\tau}{Pr} \mathcal{E}_\mathcal{G}^{t+}, \tag{10}$$

where $\mathcal{E}^+$ and $\mathcal{E}_\mathcal{G}^+$ denote, respectively, the integral mean values in the channel volume of $\overline{\omega_i^+ \omega_i^+}$ and $\overline{\vartheta_{,i^+}^+ \vartheta_{,i^+}^+}$; further, $m$ and $t$ superscripts indicate, respectively, the mean and the turbulent flow contributions to the integral dissipation rates.

Figure 1(b) displays the mean- and turbulent-flow contributions to $\overline{U}_b^+$ and $\overline{\Theta}_b^+$ across all simulated cases. For the smooth-wall flow, these contributions are estimated using the asymptotic formulations proposed in [5] and [6]. The plot illustrates how both the mean flow and turbulent fluctuations influence the overall momentum and scalar transfer, and how their relative importance evolves with increasing roughness Reynolds number. At $k^+ = 15$, the mean flow contribution surpasses that of the stochastic turbulent field. Notably, $\mathcal{E}^{t+}$ and $\mathcal{E}_\mathcal{G}^{t+}$ reach similar values, which closely match those of the smooth-wall case at the same Reynolds number. In contrast, $\mathcal{E}^{m+}$ and $\mathcal{E}_\mathcal{G}^{m+}$ are reduced relative to their smooth-wall counterparts, with $\mathcal{E}_\mathcal{G}^{m+}$ approximately 10% larger than $\mathcal{E}^{m+}$. At $k^+ = 90$, compared to smooth-wall predictions at $Re\tau = 540$, the rough-wall data shows the largest decrease in $\mathcal{E}^{m+}$, while $\mathcal{E}^{t+}$, although still significantly lower than the smooth-wall value, exceeds $\mathcal{E}^{m+}$. Meanwhile, $\mathcal{E}_\mathcal{G}^{m+}$ and $\mathcal{E}_\mathcal{G}^{t+}$ remain close in magnitude.

### *3.2 Constant flow rate (CFR)*

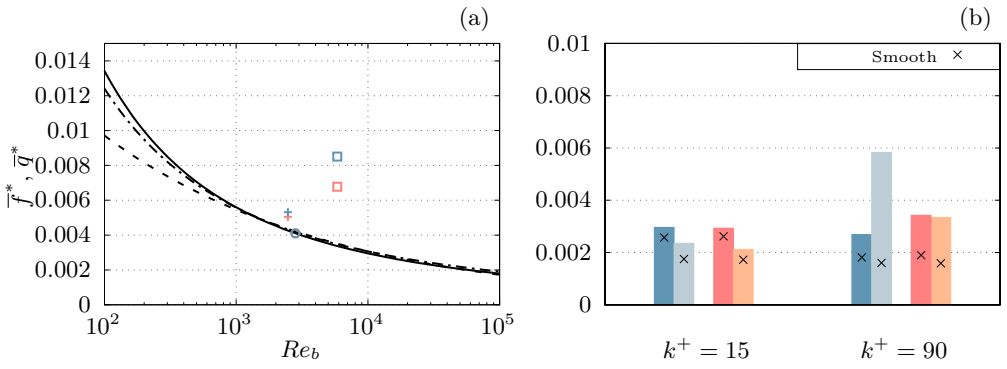


Figure 2: (a) Mean volumetric forcing (blue) and scalar source (red) terms as functions of the bulk Reynolds number. Smooth wall, circle markers; rough wall $k^+ = 15$, cross markers; rough wall $k^+ = 90$, square markers; solid line, [5]; dash-dot line, [6]; dashed line, [12]. (b) Mean and turbulent contributions to the volume-averaged dissipation rates. ■, $\mathcal{E}^{m*}/Re_b$; ■, $\mathcal{E}^{t*}/Re_b$; ■, $\mathcal{E}_\mathcal{G}^{m*}/(PrRe_b)$; ■, $\mathcal{E}_\mathcal{G}^{t*}/(PrRe_b)$.

Another common strategy for driving flow through a channel is to impose a constant flow rate (CFR). In this case, the mean bulk velocity serves as the natural velocity scale for non-dimensionalizing the problem. Using $\delta$ as the characteristic length scale, the mechanical energy balance (5) takes the form:

$$\overline{f}^* = \frac{1}{Re_b \mathcal{V}^*} \int_{\mathcal{V}^*} \overline{\omega_i^* \omega_i^*} \, \mathrm{d}\mathcal{V}^*, \tag{11}$$

where the bulk Reynolds number is $Re_b = \overline{U}_b \delta / \nu$ and a $*$ superscript denotes normalization based on $\overline{U}_b$, $\nu$, and $\delta$.

The scalar-field counterpart to driving the flow at constant flow rate (CFR) is to prescribe a constant mean bulk scalar, $\overline{\Theta}_b$. This quantity thus becomes the natural scale for non-dimensionalizing the scalar field. With this choice, the non-dimensional form of the integral balance (6) becomes:

$$\overline{q}^* = \frac{1}{PrRe_b\mathcal{V}^*}\int_{\mathcal{V}^*} \overline{\vartheta^*{}_{,i^*}\,\vartheta^*{}_{,i^*}}\,\mathrm{d}\mathcal{V}^*, \tag{12}$$

where $\overline{q}^* = q\delta/(\overline{U}_b\overline{\Theta}_b)$.

According to the CFR settings, the natural indexes for quantifying the net momentum and scalar transfer are the mean pressure gradient and the mean scalar source, $\overline{f}^*$ and $\overline{q}^*$, respectively. Hence, the Reynolds analogy factor for the CFR case becomes simply $RA = 2C_h/C_f = \overline{q}^*/\overline{f}^*$. In fact, $C_f = 2\overline{f}^*$, and $\overline{q}^*$ is $C_h = \overline{q}^*$.

The CFR scaling provides an alternative lens through which data can be analysed. Figure 2(a) presents the volumetric forcing and scalar source terms, $f^*$ and $q^*$, plotted against the bulk Reynolds number. For smooth-wall flows, the figure also includes predictions from the asymptotic momentum and scalar transfer laws of [5] and [6], as well as Dean's correlation [12] translated into the volumetric forcing $\overline{f}^*$, *i.e.* $\overline{f}^* = (1/2)\cdot 0.073\cdot(2Re_b)^{-0.25}$. To sustain a prescribed flow rate and mean scalar level, higher momentum and scalar transfer require increased forcing and source terms. Accordingly, the influence of roughness appears in figure 2(a) as high values of $f^*$ and $q^*$ relative to the smooth-wall case at the same bulk Reynolds number.

Figure 2(b) shows the mean- and turbulent-flow contributions to the mean bulk dissipation rates, $\mathcal{E}^*$ and $\mathcal{E}^*_{\mathcal{G}}$, expressed in CFR units. For both roughness cases ($k^+ = 15$ and $k^+ = 90$), all dissipation components increase relative to those of a smooth-wall flow at the same bulk Reynolds number.

At $k^+ = 15$, the deviations from smooth-wall behaviour are comparable across both the mean- and turbulent-flow contributions to mechanical energy and squared-scalar dissipation. The increase in $\mathcal{E}^{t*}$ is slightly greater than that in $\mathcal{E}^{t*}_{\mathcal{G}}$, indicating that the enhancement in momentum transfer due to roughness is somewhat stronger than the corresponding increase in scalar transfer.

At $k^+ = 90$, a significant change is observed in the turbulent contribution to mechanical energy dissipation, $\mathcal{E}^{t*}$, relative to the smooth-wall case at the same bulk Reynolds number. This suggests that the roughness-induced enhancement of momentum transfer is primarily driven by turbulence, while the mean-flow contribution, $\mathcal{E}^{m*}$, shows comparatively smaller variation. In contrast, scalar transfer exhibits similar increases in both mean- and turbulent-flow contributions to $\mathcal{E}^*_{\mathcal{G}}$ when compared to the smooth-wall reference.

The scenarios illustrated in figures 1(b) and 2(b) may appear contradictory at first: under CPG scaling, the primary roughness-induced variations in bulk dissipation rates occur in the mean-flow contributions, whereas under CFR scaling, the main changes are observed in the turbulent-flow contributions. However, this apparent discrepancy is resolved by recognizing the different interpretations, in respect to the momentum and scalar transfer, that are given to the integral dissipation rates. At CFR, equation (11) expresses the amount of mechanical energy, measured as a multiple of $\overline{U}_b^3/\delta$, that is lost to friction. The higher is this amount, the better is momentum transfer in the system. In this respect, for the $k^+ = 90$ case, figure 2(b) shows that the turbulent dissipation of mechanical energy contributes predominantly to the net amount of energy lost to friction.

According to the CPG scaling, we observe a similar scenario for the $k^+ = 90$ case in figure 1(b): the turbulent contribution to the mechanical energy dissipation is still the predominant one. However, in this case, equation (7) expresses the amount of mechanical energy, measured as a multiple of $u_\tau^3/\delta$, that the flow realizes for the given momentum flux prescribed, on average, at the channel walls. The lower is this amount of energy, the better is momentum transfer in the system.

### *3.3 Constant power input (CPI)*

A third approach for driving the flow is to supply a constant power input (CPI). CPI can be implemented in multiple ways. For example, in [13] CPI is introduced in channel-flow simulations in the context of skin-friction drag reduction analysis, defining a velocity scale corresponding to the bulk velocity of a laminar channel flow at a given pumping power. Using this velocity scale together with $\delta$ results in a non-dimensional form of the fluid momentum equation in which the resulting Reynolds number represents the prescribed power input.

In the present study, CPI is enforced differently, without introducing the laminar channel flow solution. While the laminar-based velocity scale is well defined for smooth walls, it is generally not applicable otherwise. According to the integral balance (5), CPI requires prescribing the volume-averaged dissipation

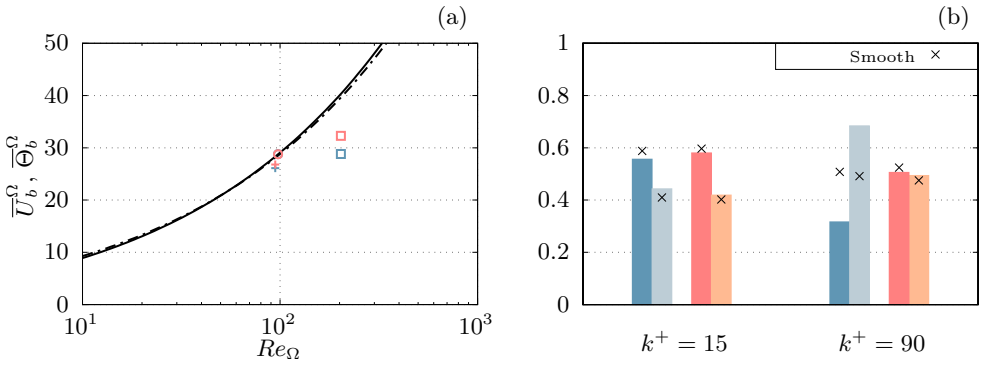


Figure 3: (a) Mean bulk velocity (blue) and scalar (red) as functions of the power Reynolds number, $Re_\Omega$. Smooth wall, circle markers; rough wall $k^+ = 15$, cross markers; rough wall $k^+ = 90$, square markers; solid line, [5]; dash-dot line, [6]. (b) Mean and turbulent contributions to the volume-averaged dissipation rates. ■, $\mathcal{E}^{m\Omega}$; ■, $\mathcal{E}^{t\Omega}$; ■, $\mathcal{E}_\mathcal{G}^{m\Omega}$; ■, $\mathcal{E}_\mathcal{G}^{t\Omega}$.

rate of mechanical energy. Therefore, CPI is implemented here by fixing the mean dissipation rate. A natural choice for a characteristic frequency scale in this context is based on $\overline{\omega_i\omega_i}$, defined as:

$$\Omega = \left(\frac{1}{\mathcal{V}}\int_\mathcal{V} \overline{\omega_i\omega_i}\,\mathrm{d}\mathcal{V}\right)^{\frac{1}{2}}, \tag{13}$$

which, together with $\nu$, allows the definition of the velocity scale, $u_\Omega = (\nu\Omega)^{1/2}$, and the length scale, $\delta_\Omega = (\nu/\Omega)^{1/2}$. With the newly introduced physical units, the power Reynolds number, $Re_\Omega = u_\Omega\delta/\nu$, can be defined.

The scalar-field counterpart of CPI is obtained by prescribing the volume-averaged dissipation rate of the squared-scalar field, $\mathcal{G}$. This is equivalent to prescribing the following quantity:

$$\Xi = \left(\frac{1}{\mathcal{V}}\int_\mathcal{V} \overline{\vartheta_{,i}\,\vartheta_{,i}}\right)^{\frac{1}{2}}, \tag{14}$$

which has the physical units of the scalar per unit length. Jointly with $\alpha$ and $u_\Omega$, it can be used to form a length scale, $\delta_\Xi = \alpha/u_\Omega$, and a scalar scale, $\vartheta_\Xi = \delta_\Xi\Xi$. Quantities made non-dimensional with $u_\Omega$, $\nu$, and $\Xi$ are denoted with an $\Omega$ superscript.

Under the CPI scaling, the friction coefficient can be written as a function of the mean bulk velocity, $C_f = 2Re_\Omega/(\overline{U}_b^{\Omega\,3})$; a similar relationship holds for the scalar transfer coefficient, $C_h = PrRe_\Omega/(\overline{U}_b^\Omega\,\overline{\Theta}_b^{\Xi\,2})$. As a result, the Reynolds Analogy factor for CPI scaled results compares the achieved mean bulk velocity and mean bulk scalar for a prescribed power input. It is given by $RA = 2Ch/C_f = Pr\left(\overline{U}_b^\Omega/\overline{\Theta}_b^\Xi\right)^2$.

Momentum and scalar transfer characteristics under CPI scaling are presented in figure 3(a), in terms of the mean bulk velocity and scalar. At matched $Re_\Omega$, the roughness-induced enhancement of momentum and scalar transfer appears as a reduction in the mean bulk velocity and scalar compared to smooth-wall flow. For a prescribed power input, the increase in the non-dimensional volumetric forcing and source terms, or equivalently, in the mean wall fluxes, is given by the reciprocal of the CPI-scaled mean bulk velocity and scalar.

Figure 3(b) shows the mean- and turbulent-flow contributions to the bulk dissipation rates for both rough-wall cases, compared with smooth-wall data at the same $Re_\Omega$. Under CPI normalization, the non-dimensional mean- and turbulent-flow contributions to each bulk dissipation rate must sum to unity. Yet the analysis of the figure is informative for understanding how the mean- and turbulent-flow contributions to the bulk dissipation rates respond to the roughness-induced increase in momentum and scalar transfer.

From figure 3(b), it is evident that, at matched $Re_\Omega$, the mechanical energy bulk dissipation behaves differently from the bulk dissipation of the squared scalar. This is most pronounced in the $k^+ = 90$ case, where $\mathcal{E}^{m\Omega}$ and $\mathcal{E}^{t\Omega}$ deviate noticeably from their smooth-wall counterparts, while $\mathcal{E}_\mathcal{G}^{m\Omega}$ and $\mathcal{E}_\mathcal{G}^{t\Omega}$ remain nearly unchanged. A similar trend is seen for $k^+ = 15$, although in this case the roughness-induced changes to $\mathcal{E}_\mathcal{G}^{m\Omega}$ and $\mathcal{E}_\mathcal{G}^{t\Omega}$ are even smaller.

## 4 Conclusions

In this work we assess the Reynolds analogy in rough wall turbulent channel flows using an energetic perspective. Following the work of Secchi et al. [1], momentum and scalar transfer are related to the integral dissipation rates of mean mechanical energy and squared scalar field; the former is defined as the sum of kinetic energy and pressure work, whereas the latter is one-half of the squared magnitude of the scalar field. The present work focuses on the interpretation of momentum and scalar transfer in fully developed channel flows when the data are normalized using velocity and length scales common to different flow driving strategies. In particular, the direct numerical simulation results presented in [1] for turbulent channel flow with random surface roughness on the channel walls are considered. Momentum and scalar transfer are analysed for two specific rough wall regimes: a transitionally rough case with a roughness Reynolds number $k^+ = 15$ and friction Reynolds number $Re_\tau = 180$, and a flow close to fully rough conditions, with $k^+ = 90$ and $Re_\tau = 540$. Data from these rough wall cases are compared with smooth wall reference conditions estimated using momentum and scalar transfer laws available in the literature [5, 6]. For the scalar transfer a unit Prandtl number is considered throughout the study. Three different flow driving conditions are investigated: the constant pressure gradient (CPG), the constant flow rate (CFR), and the constant power input (CPI) approaches.

For the CPG case, natural indexes for assessing momentum and scalar transfer are the non-dimensional mean bulk velocity and scalar, $\overline{U}_b^+$ and $\overline{\Theta}_b^+$. At fixed friction Reynolds number, a more effective momentum and scalar transfer manifests itself through low values of $\overline{U}_b^+$ and $\overline{\Theta}_b^+$ in the channel. Hence, roughness improves both momentum and scalar transfer as it determines a decrease in both these quantities with respect to smooth wall conditions; in particular, the decrease in $\overline{U}_b^+$ exceeds that in $\overline{\Theta}_b^+$ as a manifestation of a more emphasized momentum transfer in comparison to the scalar one. In terms of the integral dissipation rates, the analysis shows that for the lowest $Re_\tau$ case, *i.e.* the case with $k^+ = 15$, the roughness-induced momentum and scalar transfer enhancement appears through a decrease in the mean flow contribution of the integral dissipation rates. In contrast, for the highest $Re_\tau$ case, *i.e.* the $k^+ = 90$ case, momentum transfer is significantly impaired by the contribution of the dissipation of turbulent fluctuations in the channel. At the same time, the net scalar transfer is approximately equally affected by the mean and turbulent flow integral dissipations.

At CFR the natural indexes for measuring the net momentum and scalar transfer in the channel are the non-dimensional mean pressure gradient and scalar source, respectively $f^*$ and $q^*$, that are required to drive the flow and the scalar field. Increases in momentum and scalar transfer in the channel are observed as increases in these two quantities. Hence, the roughness-induced enhancement of momentum and scalar transfer is observed in the present CFR-scaled data as an increase of $f^*$ and $q^*$ in comparison to smooth wall data at matched bulk Reynolds number. For the lowest Reynolds number case, *i.e.* at $k^+ = 15$, the increase in momentum and scalar transfer manifests itself approximately equally as an increase the mean- and turbulent-flow integral dissipation rates of mechanical energy and squared scalar field. For the highest bulk Reynolds number case, *i.e.* at $k^+ = 90$, the roughness-induced momentum transfer enhancement appears predominantly through an increase in the turbulent contribution to the integral dissipation of mechanical energy with respect to smooth wall conditions at matched bulk Reynolds number. In contrast, changes in the mean- and turbulent-flow integral dissipation of the squared scalar field appear to be similar.

A third flow-driving strategy considered in this study is supplying the flow with a constant power input (CPI). Unlike previous approaches in the literature [13, 7], CPI is implemented here by prescribing the channel-volume average of $\overline{\omega_i \omega_i}$. An analogous strategy for the scalar transfer problem is obtained by fixing $\overline{\vartheta_{,i}\, \vartheta_{,i}}$. Specifying these quantities, together with the molecular diffusivities of the fluid, defines new characteristic velocity, length, and scalar scales that enable rescaling of the data according to CPI normalization.

Under CPI conditions, the mean bulk velocity varies inversely with the required volumetric forcing: an increase in momentum transfer appears as a reduction of the mean bulk velocity accompanied by a rise in the volumetric driving force. A corresponding behaviour is observed for scalar transfer enhancement, where a decrease in the mean scalar value is paired with an increase in the required volumetric scalar source term.

**Acknowledgments**

We greatly acknowledge the support by the German Research Foundation (DFG) under the Collaborative Research Centre TRR150 (project number 237267381). The simulations presented in this work were performed on the HPE Apollo (Hawk) supercomputer at the High Performance Computing Center Stuttgart (HLRS) under the grant number 44198

## References

[1] F. Secchi, D. Gatti, U. Piomelli, and B. Frohnapfel. A framework for assessing the Reynolds analogy in turbulent forced convection over rough walls. *J. Fluid Mech.*, 1006:R3, 2025.

[2] Z. Hantsis and U. Piomelli. Numerical simulations of scalar transport on rough surfaces. *Fluids*, 9(7), 2024.

[3] K. Fukagata, K. Iwamoto, and N. Kasagi. Contribution of Reynolds stress distribution to the skin friction in wall-bounded flows. *Phys. Fluids*, 14(11):L73–L76, 11 2002.

[4] Y. Hasegawa and N. Kasagi. Dissimilar control of momentum and heat transfer in a fully developed turbulent channel flow. *J. Fluid Mech.*, 683:57–93, 2011.

[5] H. Abe and R. A. Antonia. Relationship between the energy dissipation function and the skin friction law in a turbulent channel flow. *J. Fluid Mech.*, 798:140–164, 2016.

[6] H. Abe and R. A. Antonia. Relationship between the heat transfer law and the scalar dissipation function in a turbulent channel flow. *J. Fluid Mech.*, 830:300–325, 2017.

[7] M. Quadrio, B. Frohnapfel, and Y. Hasegawa. Does the choice of the forcing term affect flow statistics in dns of turbulent channel flow? *Eur. J. Mech. B Fluids*, 55:286–293, 2016. Vortical Structures and Wall Turbulence.

[8] M. Thakkar, A. Busse, and N. Sandham. Surface correlations of hydrodynamic drag for transitionally rough engineering surfaces. *J. Turb.*, 18(2):138–169, 2017.

[9] M. Thakkar. *Investigation of turbulent flow over irregular rough surfaces using direct numerical simulations*. PhD thesis, University of Southampton, October 2017.

[10] M. Thakkar, A. Busse, and N. D. Sandham. Direct numerical simulation of turbulent channel flow over a surrogate for Nikuradse-type roughness. *J. Fluid Mech.*, 837:R1, 2018.

[11] J. W. R. Peeters and N. D. Sandham. Turbulent heat transfer in channels with irregular roughness. *Int. J. Heat Mass Transf.*, 138:454–467, 2019.

[12] R. B. Dean. Reynolds number dependence of skin friction and other bulk flow variables in two-dimensional rectangular duct flow. *J. Fluids Eng.*, 100(2):215–223, 06 1978.

[13] Y. Hasegawa, M. Quadrio, and B. Frohnapfel. Numerical simulation of turbulent duct flows with constant power input. *J. Fluid Mech.*, 750:191–209, 2014.